IEEE ROBOTICS AND AUTOMATION LETTERS. PREPRINT VERSION. ACCEPTED *DECEMBER*, *2017*

Lightweight, high-force gripper inspired by chuck clamping devices

Toshihiro Nishimura[1], *Student Member, IEEE*, Masanari Tennomi[1], *Student Member, IEEE*, Yosuke Suzuki[2], *Member, IEEE,* Tokuo Tsuji[2], *Member, IEEE*, and Tetsuyou Watanabe[2], *Member, IEEE*

***Abstract*—In this paper, we present a novel gripper, whose design was inspired by chuck clamping devices, for transferring heavy objects and assembling parts precisely in industrial applications. The developed gripper is lightweight (0.9 kg), can manipulate heavy payloads (over 23 kgf), and can automatically align its position and posture via a grasping motion. A fingertip design criterion is presented for the position alignment, while a control strategy is presented for the posture alignment. With one actuator, this gripper realized the above features. This paper describes the mathematical analyses and experiments used to validate these key metrics.**

***Index Terms*— Grippers and Other End-Effectors, Grasping, Mechanism Design, Underactuated Robots, Assembly**

I. Introduction

MANY robotic grippers [1][2] have been developed for the purpose of factory automation. The grippers' primary functions are transferring and assembling parts or products. In these operations, the preferable functional requirements for the gripper are as follows: 1) it must be able to generate high force to grasp objects stably and transfer heavy objects; 2) it must be lightweight relative to the payload of manipulator; and 3) its position and posture must automatically align appropriately for precise assembly via a grasping motion. This paper presents a novel gripper that satisfies these three requirements.

In industrial applications, robotic grippers must accommodate large payloads (i.e., weight of the grasped object) and grasping forces. In general, large actuators or transmissions are needed to construct high force gripper, resulting in heavy gripper designs; there is a direct relationship between payload magnitude and weight. Nonetheless, a lightweight, high-force gripper design is preferable. In assembly processes, the precise alignment of the gripper's position and posture is necessary to ensure high processing speed and smooth operation.

Many common parts, such as gears and shafts, are cylindrical in shape. Thus, the gripper described in this paper was developed to manipulate cylindrical objects. Drilling and turning machines utilize chuck devices to grasp cylindrical tools. Inspired by these chuck devices, we developed a lightweight, high-force gripper as shown in Fig. 1. The feed screw mechanism transduces motor torque into a large driving force, which generates a large grasping force. Even when interrupting the electric supply to the motor, the grasping force is maintained by the self-locking property of the screw. The developed prototype gripper has a weight of 0.9 kg and its payload is over 23 kgf. As shown in Fig. 1, the gripper has two grasping modes. One drawback of the chuck-based gripper design is its narrow space for grasping, which makes it difficult to grasp wide objects. Therefore, the expanded mode shown in Fig. 1(b) was implemented to grasp objects that were too wide to be grasped in the normal mode shown in Fig. 1(a). In the expanded mode, the fingers protrude outside of the cover to provide a wide space for grasping. In both modes, the fingers close towards the center of the gripper in synchrony, and the position and posture of the grasped object can be automatically aligned.

(a) Normal mode (b) Expanded mode

Figure 1. Developed gripper

A. Related work

Many types of robotic hand devices have been produced [3], including for the purpose of producing high forces[4]–[18], similar to the goal of this study. Table I lists the related specifications for these high-force robotic hands. The SLUM gripper [14], flexible gripper [15], and Multi-DOF hand [16] designs can maintain large grasping forces without an electric supply, by utilizing rocking mechanisms. We defined a payload-to-weight ratio calculated by dividing the payload by the weight of the device, to evaluate the largest obtainable payload at the lowest possible weight. When handling an object with a gripper attached to a manipulator, the summation of the weights of the object and gripper must be under the given payload for the manipulator. A large payload-to-weight ratio maximizes the payload for a given manipulator. In this context, the gripper developed in our present study attained the best performance, as shown in Table I.

Manuscript received: September, 10, 2017; Revised December, 2, 2017; Accepted December, 24, 2017.

This paper was recommended for publication by Editor Han Ding upon evaluation of the Associate Editor and Reviewers' comments. This work was supported by NEDO Project P17004.

[1]T. Nishimura and M. Tennomi are with the Graduated school of Natural science and Technology, Kanazawa University, Kakuma-machi, Kanazawa, 9201192 Japan (e-mail: to.nishimura@stu.kanazawa-u.ac.jp).

[2]Y. Suzuki, T. Tsuji, and T. Watanabe are with the Faculty of Mechanical Engineering, Institute of Science and Engineering, Kanazawa University, Kakuma-machi, Kanazawa, 9201192 Japan (e-mail: te-watanabe@ieee.org).

Digital Object Identifier (DOI): see top of this page.

In assembly processes, the precise alignment of parts is necessary, and several approaches have been used to achieve automatic alignment during assembly. Zhang et al. proposed an algorithm for aligning the posture of a part with parallel-jaw grippers [19][20]. Harada et al. proposed a strategy in which the position and posture of an object on a table were aligned by utilizing two passively and two actively moving fingers [21]. Dobashi et al. proposed a strategy for assembling parts whose position and posture were uncertain, with four cylindrical fingers [22]. Hirata et al. proposed a design in which the gripper mechanisms were capable of automatic part alignment [23][24]. This study also challenges to embed the automatic part alignment function in the gripper. A fingertip design method is presented for the position alignment, while a control strategy is presented for the posture alignment.

TABLE I. SPECIFICATIONS AND PERFORMANCE; THE DEVELOPED GRIPPER AND RELATED ROBOTIC HANDS

	Weight [kg]	Fingertip force [N]	Payload [kgf]	Payload-to-weight ratio[-]*
DLR Hand II [4][5]	1.8	30	4.9**	2.7
Robotiq 3-Finger gripper [6]	2.3	60	10	4.3
Barrett Hand [7][8]	0.98	-	6.0	6.1
Tokyo-TECH 100N Hand [10]	0.94	100	12.2**	13.0
FRH-4 hand[13]	0.22***	-	11.2	-****
SLUM gripper [14]	3.5	-	10	2.9
Flexible gripper [15]	2.61	-	4.0	1.5
Multi-DOF hand [16]	2.4	113	50	20.8
Underactuated soft gripper [17]	0.7	-	3.0	4.3
Jamming gripper (3.5" Head) [18]	0.64***	-	4.5	-****
Developed gripper	0.9	**350**	Over 23	**25.6**

The bold value indicates the best performance in each metric.

* Payload-to-weight ratio: Payload/Weight

** The payload was not presented, and the value was calculated by the multiplication of the fingertip force, number of fingers, and friction coefficient (0.4)

*** The weight did not include air supply devices

**** We did not calculate these values because the weight did not include air supply devices

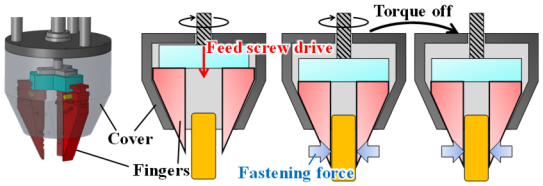

Figure 2. Schematic view of the main mechanism based on chuck device

II. GRIPPER DESIGN.

A. *Functional requirements*

To ensure the gripper would be suitable for use in industrial tasks, such as product assembly, the functional requirements of the gripper were set as follows:

1. The payload of the gripper must be greater than 196 N (20 kgf).
2. The weight of the gripper must be less than 1.0 kg.
3. The gripper must be able to grasp objects with a width greater than 100 mm.
4. Position and posture alignments must be automatically performed via a grasping motion.
5. The gripper must be able to grasp cylindrical parts, with radial symmetry.

We designed the gripper to satisfy the requirements in the normal or expanded mode.

B. *Main mechanism*

Based on the mechanism of chuck device, we adopted the mechanism shown in Fig. 2, where the three fingers close with being pushed out owing to the feed screw mechanism and constraint by the cover. The feed screw mechanism transduces the motor torque into a high driving force to ensure a large grasping force. Similarly to chuck device, the gripper can maintain a large grasping force without electric supply by the self-locking property of the screw. As shown in Fig. 2, the fingers are radially arranged at regular intervals on a circle, and their closing motion facilitates automatic alignment of the position and posture of the part.

C. *Structure*

Fig. 3 shows the CAD models for the developed gripper. The gripper mainly consists of the three fingers (red parts in Fig. 3), the finger base (light blue part in Fig. 3), the cover, the servomotor (Dynamixel, XM430-W210), the 6 guide rails, and the feed screw mechanism. The fingers are mounted on the finger base and constrained by the guide rails so that the fingers can slide in the direction of opening and closing of the gripper. Fig. 3(b) shows the finger structure. The finger pad is beveled for the automatic alignment and grasping of small objects. The phalange and base are connected through torsion spring, and the phalange is abducted if the constraint of the cover is removed. The finger surface is knurled for increasing friction so that an object can be easily grasped especially at the expanded mode. The guide rails are mounted on the inside of the cover, as shown in Fig. 3(c). The slide pin at the finger base (yellow parts at Fig. 3(b)) slides along the guide rails for converting the straight motion of the feed screw into the opening and closing motions of the gripper or fingers (See Fig. 3(c)). Fig. 4(a) shows the schematic view of the motions of the shafts, finger base, and fingers at the normal mode. The outer shaft with internal screw thread is attached to the servomotor, while the finger base is attached on the tip of the inner shaft with external screw thread. The rotational motion of the outer shaft by the servomotor drives the straight motion of the inner shaft and finger base. As shown in Fig. 4, the fingers are pushed out (pulled in) by the straight motion of the finger base, and opened (closed). With this structure, even when opening and closing the gripper, the position of the servomotor does not change, which is preferable for the durability of motor and wiring. The three fingers close, moving the same distance to approach the center of the gripper, and the position of the part is aligned at the center while its posture is aligned so that the longitudinal direction of the part coincides with that of the fingers. The maximum width of graspable object at the normal mode is 42 mm. To grasp an object whose width is over the maximum width, the expanded mode is adopted. If the pushing of the finger base is continued after finishing the closing of fingers at the normal mode, the constraint by the cover is released and the fingers are protruded owing to the torsion springs, as shown in Fig. 4(b). If the finger base is pulled from this state, the protruded fingers close owing

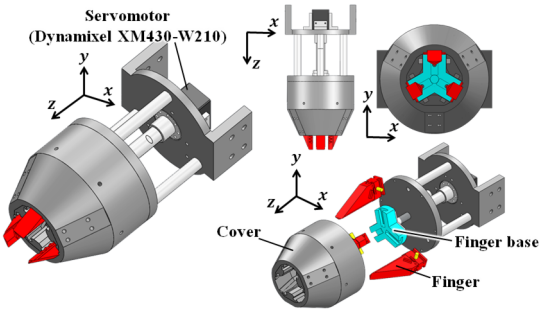

(a) CAD models of the developed gripper

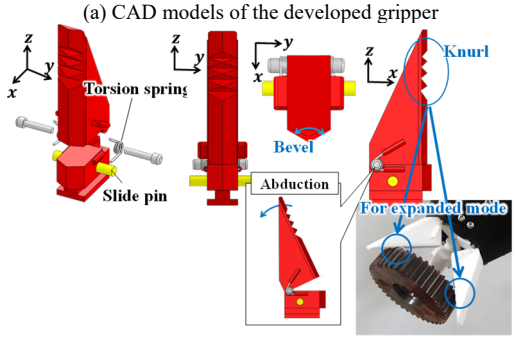

(b) CAD models of the finger

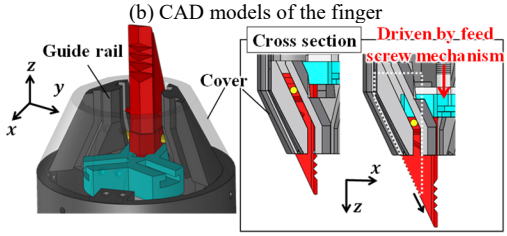

(c) Structure of the guide rail for one finger (Two guide rails for one finger)

Figure 3. CAD models of the developed gripper and the structure of the finger

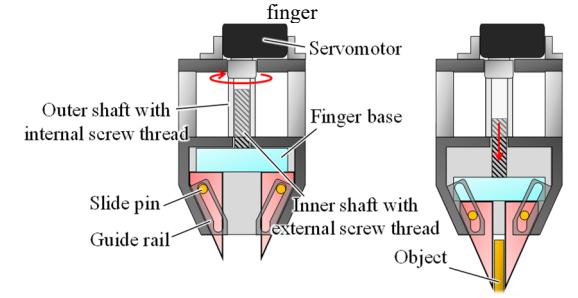

(a) Normal mode

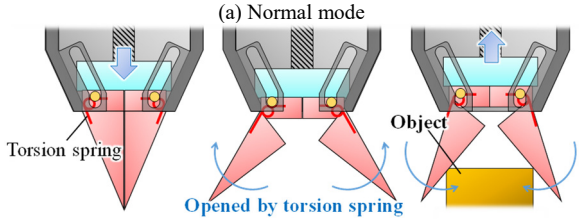

(b) Expanded mode

Figure 4. Schematic view of the motions at each mode

to the constraint resulting from the contact between the cover and the rear side of the fingers. With this mechanism, wide objects can be grasped at the expanded mode.

III. Position And Posture Alignment Mechanism

A. Position alignment

As shown in Fig. 5, the closing motion provides the position alignment. The angle of the bevel ϕ_a shown in Fig. 6 has an important role in the position alignment. This section describes the derivation of ϕ_a. For simplicity, the shape of the object was assumed to be cylindrical, and the object was located on a slippery table. Planar analysis was conducted. If an object is not centered, the following steps are traced with the closing of the fingers (Fig. 5). Step 1: the object contacts one finger first. Step 2: the object comes in contact with two fingers. Step3: the object contacts all the three fingers and becomes centered. Note that it is possible that step1 is skipped. When contacting only one finger, the object slides on the table. On the other hand, when contacting two fingers, it is possible that the sliding of the object stops and the position alignment fails. Therefore, we consider the case when a cylindrical object contacts two fingers, as shown in Fig. 6. It is noted that we do not consider the situation where the gripper loses its hold on the object during the closing, because the grasp planning is beyond the scope of this study. $\boldsymbol{f}_{ni}$ and $\boldsymbol{f}_{ti} (i \in \{1,2\})$ denote the normal and tangential components of the force applied to the object by finger i, respectively. $\boldsymbol{f}_{\mathrm{fri}}$ denotes the static maximum (kinetic when sliding) frictional force applied to the object from the table, and its direction is opposite to that of the resultant force $\sum_{i=1}^{2}(\boldsymbol{f}_{ni} + \boldsymbol{f}_{ti})$. The coordinate frame Σ_A was set so that x_A axis could be parallel to the direction of $\sum_{i=1}^{2}(\boldsymbol{f}_{ni} + \boldsymbol{f}_{ti})$ and its positive direction would be toward the center of the gripper. Let ϕ_b be the angle between y_A axis and the contact tangential direction. We will analyze the system by taking into account the symmetry with respect to the x_A axis.

The condition for realizing the position alignment is that the object continues moving/sliding until it reaches the center of the gripper. The condition is then written as

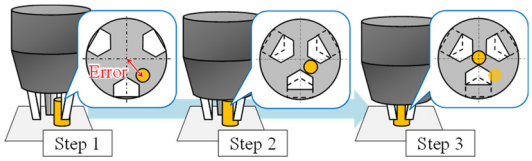

Figure 5. Schematic view of the position alignment

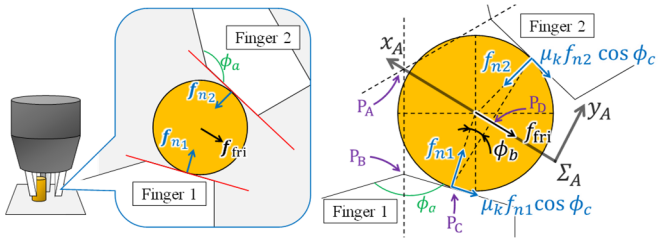

(a) Forces applied to the object (b) Zoomed-up view for the other setting

Figure 6. Model for the analysis of the position alignment

$$\left\| \boldsymbol{e}_x^{\mathrm{T}} \sum_{i=1}^{2} (\boldsymbol{f}_{ni} + \boldsymbol{f}_{ti}) \right\| = \|\boldsymbol{f}_{\mathrm{fri}}\| \tag{1}$$

$$\boldsymbol{e}_x^{\mathrm{T}} \sum_{i=1}^{2} (\boldsymbol{f}_{ni} + \boldsymbol{f}_{ti}) > 0 \tag{2}$$

where $\boldsymbol{e}_x$ denotes the unit vector along the positive x_A axis. When closing the fingers, they are pushed out in the positive z_A direction by the feed screw. Accordingly, the tangential contact force is large while the normal contact force is small at the contact point between the object and each finger. Therefore, the contact can be regarded as a kinetic friction state. If the contact

is not the kinetic friction state, the closing motion of the gripper stops and the object cannot be grasped. Taking μ_k as the kinetic frictional coefficient at the contact point between the object and the fingers, the magnitude of the tangential component of the contact force applied from finger i is given by $\|\boldsymbol{f}_{ti}\| = \mu_k \|\boldsymbol{f}_{ni}\|$. Then, considering the symmetry of the system and then $\|\boldsymbol{f}_{\mathrm{n1}}\| = \|\boldsymbol{f}_{\mathrm{n2}}\|$, (1) and (2) can be rewritten by

$$2\|\boldsymbol{f}_{\mathrm{n1}}(\sin\phi_b - \mu_k \cos\phi_c \cos\phi_b)\| = \|\boldsymbol{f}_{\mathrm{fri}}\| \tag{3}$$

$$\sin\phi_b - \mu_k \cos\phi_c \cos\phi_b > 0 \tag{4}$$

where $\mu_k \cos\phi_c \|\boldsymbol{f}_{ni}\|$ is the magnitude of the mapped $\boldsymbol{f}_{ti}$ on the $x_A y_A$ plane (ϕ_c is the angle between $x_A y_A$ plane and $\boldsymbol{f}_{ti}$). Since a slippery table is assumed, $\|\boldsymbol{f}_{\mathrm{fri}}\|$ is small. Additionally, $\|\boldsymbol{f}_{\mathrm{n1}}\|$ would increase until (3) can be satisfied if (4) is held, and the closing motion then continues. Therefore, we only have to satisfy (4) for the position alignment. From the relation between the inner angles of the quadrangle $\mathrm{P_A P_B P_C P_D}$ shown in Fig. 6(b), we get $\phi_b = \phi_a/2 - 60°$. Moreover, $1 \geq \cos\phi_c \geq 0$.Then, the sufficient condition for satisfying (4) is

$$\phi_b > \tan^{-1}\mu_k \quad or \quad \phi_a > 120° + 2\tan^{-1}\mu_k \tag{5}$$

This is the condition for ϕ_a for realizing the position alignment. Assuming that the materials for the object and fingers are plastic (PLA), the kinetic frictional coefficient can be set as $\mu_k = 0.2$. Then, we set $\phi_a = 145°$ considering the manufacturing error.

We investigated the function of position alignment by using the fingers with $\phi_a = 145°$. The experimental setup is shown in Fig. 7. The objects were cylinders with a diameter of 10, 20, and 25 mm and cuboid with the 20mm square bottom face. The nominal closing speed was 0.8 mm/s and we also investigated the case when the speed was 0.4 mm/s for comparison (Note that the available speed was 0~0.8 mm/s).

Let $\boldsymbol{x}_{\mathrm{obj}} = [x_{\mathrm{obj}}, y_{\mathrm{obj}}]^{\mathrm{T}}$ be the geometrical center of the base of the object captured by the camera, $\boldsymbol{x}_{\mathrm{c}} = [x_c, y_c]^{\mathrm{T}}$ be the center of the gripper, derived by considering it to correspond to the geometrical center of the triangle constructed by connecting the three apexes of the fingertips captured by the camera at the initial state. Here, we define the following position error of the object.

$$\boldsymbol{x}_e = \boldsymbol{x}_{\mathrm{obj}} - \boldsymbol{x}_c \tag{6}$$

Fig. 8 shows the experimental results of the cylinder with a dimeter of 20 mm giving the overview of the position alignment and time series data of $\|\boldsymbol{x}_e\|$. We conducted over 30 experiments for each object by changing the initial object position $\boldsymbol{x}_0$ randomly. If $\|\boldsymbol{x}_e\|$ converged to less than 1 mm, we judged the position alignment to be successful. In Fig. 9, the red and blue makers show the initial positions for success and failure cases, respectively. Fig. 9(a) illustrates that the position alignment function works well if the initial position error $\|\boldsymbol{x}_{e_0}\|(= \|\boldsymbol{x}_{\mathrm{obj}_0} - \boldsymbol{x}_c\|)$ is less than 10.3, 12.8 and 15.7 mm for the cylinders with the diameter of 10, 20, and 25 mm, respectively. In Fig. 9(b), the distribution of the red maker (success case) was not uniform. As suggested/implied by (5), the alignment function does not work if the angle between the sides of the object and fingertips (ϕ_b) is small. The angle varies

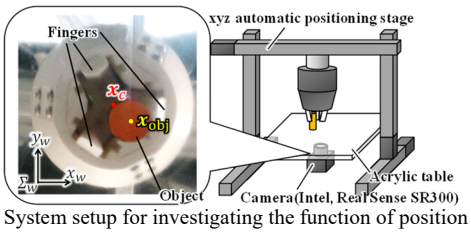

Figure 7. System setup for investigating the function of position alignment

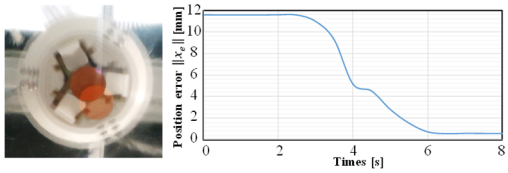

(a) Composited image of the initial and final positions (b) Time series data of the position error $\|\boldsymbol{x}_e\|$

Figure 8. Representative data of position alignment test

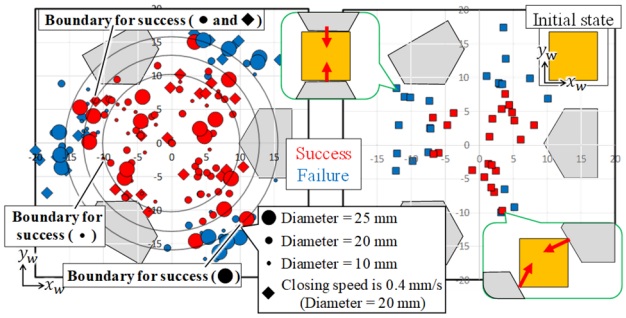

(a) Cylinders with different diameters (b) Cuboid

Figure 9. Experimental results of the position alignment

with the initial position of cuboid. This is the reason for the non-uniform results. The results also indicates the effect of initial orientation of the object. No effect of different speeds was observed.

B. Posture alignment

As shown in Fig. 10, the posture is aligned when grasping the cylindrical object even when the initial posture is different from the aligned posture, where the longitudinal direction of the object coincides with that of the fingers. The posture alignment fails only when the rotational motion of the object stops before the alignment completes. The problematic rotation is the rotation around the y_w (y_G) axis shown in Figs. 10 and 11, because the allowable rotational direction is only positive, and then the rotation could stop, due to the constraint by the table. Therefore, we focus on the rotation around the contact point 1 ($\mathrm{C_1}$) on finger 1 at the $z_w x_w$ plane and try to positively rotate the object at $\mathrm{C_1}$ around the y_w axis without stopping before completion, which leads to the posture alignment. It is noted that the sliding at $\mathrm{C_1}$ does not contribute directly to the posture alignment. The velocities of fingers 1 and 2 at the closing motion are given by

$$\begin{aligned}\boldsymbol{v}_{f1} &= \begin{bmatrix} v_{f1_x} \\ v_{f1_z} \end{bmatrix} = N_m p \begin{bmatrix} -C_{\mathrm{grp}} + S_{\mathrm{grp}} T_f \\ -S_{\mathrm{grp}} - C_{\mathrm{grp}} T_f \end{bmatrix} \\ \boldsymbol{v}_{f2} &= \begin{bmatrix} v_{f2_x} \\ v_{f2_z} \end{bmatrix} = N_m p \begin{bmatrix} -C_{\mathrm{grp}} - S_{\mathrm{grp}} T_f \cos 60° \\ -S_{\mathrm{grp}} + C_{\mathrm{grp}} T_f \cos 60° \end{bmatrix}\end{aligned} \tag{7}$$

where $C_{\mathrm{grp}} = \cos\theta_{\mathrm{grp}}$, $S_{\mathrm{grp}} = \sin\theta_{\mathrm{grp}}$, $T_f = \tan\theta_f$, θ_f is the taper angle of the finger, N_m is the rotational frequency and $N_m > 0$ when the motor positively rotates, p is the pitch of the feed screw (See Fig. 11).

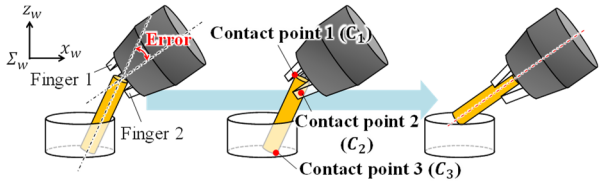

Figure 10. Schematic view of the posture alignment

The aim of the strategy is to control finger 1 so that C_1 can be fixed with respect to the table (or base frame), when closing the finger/gripper. The fixing of C_1 indicates that the allowable motion of the object is the rotation around C_1, while C_2 moves toward the positive z_w and negative x_w directions via the closing motion of the fingers ($\boldsymbol{v}_{f2} - \boldsymbol{v}_{f1} = 3N_m p T_f / 2\left[-S_{\mathrm{grp}}, C_{\mathrm{grp}}\right]^T$). The motion of C_2 provides a positive rotation around C_1, which indicates that C_3 moves toward the direction where C_3 is detached from the table. Then, the posture alignment can work. It is noted that it is possible that the rotation around C_1 by the velocity (motion) of C_2 ($\dot{\theta}_{C1}^{C2}$) could be negative when the x_w coordinate of C_2 is larger than that of C_1 because the object angle (θ_{obj}) is large. In this case,
$\dot{\theta}_{C1}^{C2} = 3l_{12}N_m p \mathrm{T_f}/2\sin\left(\theta_{\mathrm{grp}} + \tan^{-1}(l_{c2}/(d+d_c)) - \theta_{\mathrm{obj}}\right)$
where l_{12} is the distance between C_1 and C_2. The definitions for the other variables are shown in Fig. 15. Then, the condition for $\dot{\theta}_{C1}^{C2} > 0$ is $\theta_{\mathrm{grp}} + \tan^{-1}(l_{c2}/(d+d_c)) > \theta_{\mathrm{obj}}$. If assuming that the object is thin, $l_{c2} \gg (d+d_c)$ and then $\dot{\theta}_{C1}^{C2} > 0$ is always held. We move the gripper (xyz-stage) with a speed of $-\boldsymbol{v}_{f1}$ while closing it so that C_1 can be fixed with respect to the table. It is remarked that the setting of $-\boldsymbol{v}_{f1}$ assumed that there was no sliding at C_1. Practically, the sliding could occur and we could compensate the sliding motion by adding the compensation term at $-\boldsymbol{v}_{f1}$. However, another sensor such as a camera is required for the compensation and then it will not be cost-effective. Additionally, even if the sliding occurs, we can apply the strategy by regarding C_1 as the one that should be fixed when the sliding stops. There are several concave areas on the surface of the fingers, and the sliding stops with high possibility when C_1 reaches the area. Therefore, we took this easy control strategy.

Here, we investigated the available range for the posture alignment. Fig. 12 shows the experimental setup. A cup was utilized to set the initial posture of the object. Taking $\theta_{\mathrm{obj_0}}$ and $\theta_{\mathrm{grp_0}}$ as the initial postures of the object and gripper, respectively, we defined the initial posture error of the object:

$$\theta_{e0} = \theta_{\mathrm{obj_0}} - \theta_{\mathrm{grp_0}} \tag{8}$$

To prevent the collision between the object and table after the posture alignment, we set $\theta_{\mathrm{obj_0}}$ such that $\theta_{\mathrm{obj_0}} > \theta_{\mathrm{grp_0}}$. We split the range of θ_{e0} into the incremental ranges, each spanning 5°, and repeated the investigation by randomly selecting $\theta_{\mathrm{obj_0}}$ until the number of trial times for each range was more than three. Fig. 13 shows the success rate, and Fig. 14 shows the snapshots for the successful case. Fig. 13(b) shows the case utilizing the strategy. A success rate of 100% was obtained in all the ranges, which shows the validity of the proposed control strategy. Fig. 13(a) shows the case when the strategy is not utilized. The posture alignment failed when θ_{e0}, namely, θ_{obj} for constant θ_{grp} was large. Here, we discuss the reason. Fig. 15 shows the model for the analysis, where each unilateral arrow shows the positive direction for each corresponding variable. Let m_{C1y} be the moment around the y_w axis, and f_{gi_n}, f_{gi_t} be the normal and tangential contact forces, respectively, at C_i ($\in \{1,2,3\}$). Then, the condition for accelerating the positive rotation can be written as

$$m_{C1y} = \alpha_1 f_{g2_n} - \alpha_2 f_{g3_n} - \alpha_3 m_o g > 0 \tag{9}$$

where

$$\alpha_1 = l_{c2}\cos\psi - \mu_{\mathrm{o}}(d + d_c)$$
$$\alpha_2 = \sqrt{l^2 + 4d^2}(\mu_r \sin\zeta - \cos\zeta)$$
$$\alpha_3 = l_g \cos\left(\theta_{\mathrm{obj}} + \theta_{cg}\right)$$
$$\zeta = \theta_{\mathrm{obj}} + \tan^{-1}\frac{2d}{l},\ f_{g2_n} \geq 0,\ f_{g3_n} \geq 0$$

Here, $f_{g2_n}\cos\psi$ is the mapped f_{g2_n} on the $z_w x_w$ plane, θ_{obj} is the posture of the object, $m_o g$ is the gravity term, and μ_{o} and μ_r are the ratio of the magnitude of frictional force to the normal force at the contact points between the object and fingers, and the object and table, respectively. Taking μ_{om} and μ_{rm} as the maximum frictional coefficients at the contact points, we get $\mu_{\mathrm{o}} \leq \mu_{\mathrm{om}}$ and $\mu_r \leq \mu_{rm}$. If the diameter of the object is

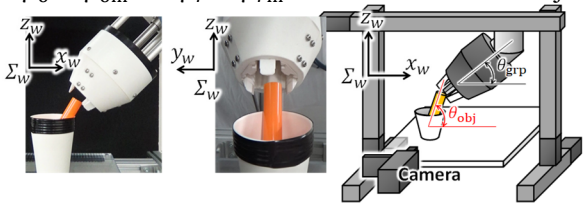

Figure 12. System setup for testing the function of the posture alignment

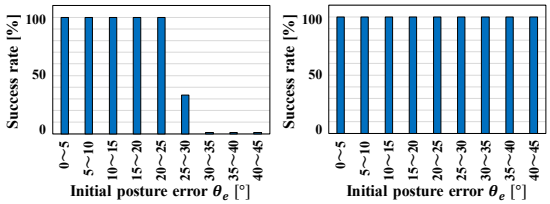

(a) Without control (b) With control
Figure 13. Experimental results: initial posture error θ_e versus the success rate of the posture alignment

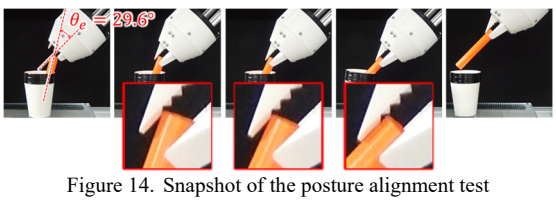

Figure 14. Snapshot of the posture alignment test

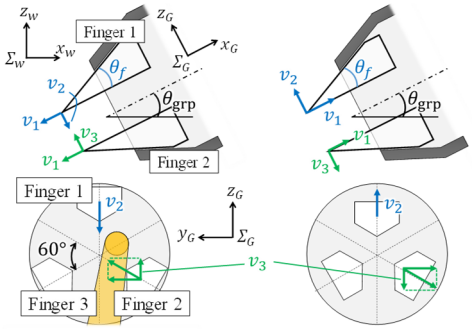

(a) When closing ($N_m > 0$) (b) When opening ($N_m < 0$)
Figure 11. Direction of the velocity of the fingertip in the posture alignment strategy: N_m is the rotational frequiency and p is the pitch of the feed screw. ($v_1 = N_m p, v_2 = N_m p \tan\theta_f, v_3 = N_m p \tan\theta_f \cos 60°$)

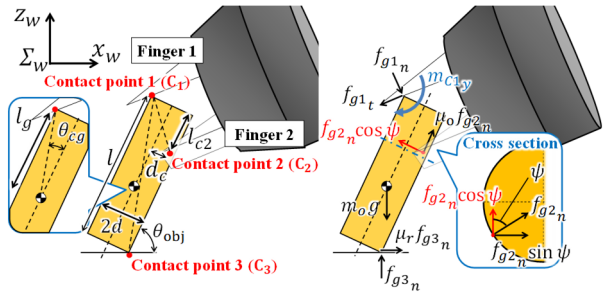

(a) Geometrical representations (b) Statics

Figure 15. Model for analyzing the posture alignment

small ($l_{c2} \gg (d + d_c)$) and μ_o is small, we get $\alpha_1 > 0$. Here, $m_o \approx 0$ is assumed. Then, if θ_{obj} is small ($\theta_{\text{obj}} < -\tan^{-1}(2d/l) + \tan^{-1}(1/\mu_r) = 67°$ for $d = 7.5$ mm, $l = 130$ mm, $\mu_r = 0.3$), $\alpha_2 < 0$ and then $m_{\text{C1y}} > 0$ (9) can be satisfied irrespective of the values of ${f_{gi}}_n$ ($i \in \{2,3\}$). Note that $\theta_{\text{obj}} < 68°$ corresponds to $\theta_e < 23°(= 68° - \theta_{\text{grp}}(= 45°))$. If θ_{obj} is not small, it is possible that $m_{\text{C1y}} \leq 0$ and the motion for the posture alignment stops before completion. This is the reason for the failure results shown in Fig. 13(a). From (9), ${f_{g3}}_n$ should be small for $m_{\text{C1y}} > 0$. It is noted that ${f_{g3}}_n = 0$ indicates the case when losing the contact with the table, and then $m_{\text{C1y}} > 0$ is always satisfied under the condition of $\alpha_1 > 0$. In other words, $\alpha_1 > 0$ ($l_{c2}\cos\psi > \mu_o(d + d_c)$) is the condition for $m_{\text{C1y}} > 0$ when losing contact with the table.

IV. Feasibility Study

This section shows the maximum payload (weight of graspable object) by the developed gripper.

A. Analysis

As shown in Fig. 16, the target is a cylindrical object and we will derive the maximum weight of the graspable object at the expanded mode. Because of cylindrical symmetry, we consider the half section of the system as shown in Fig. 16. The maximum payload at the normal mode can be regarded as the one in the case where the angle between the object and finger, θ_{g} (Fig. 16(b)), is zero. Because the problem is indeterminate, we will formulate it as an optimal problem for power grasp [25][26] and then solve it.

Let ${f_{m_n}}, {f_{m_t}}, {f_{\text{frm}_n}}, {f_{\text{frm}_t}}, f_{\text{obj}}$, and $\mu_{\text{om}} f_{\text{obj}}$ be the normal and tangential forces at each contact point, as shown in Fig. 16,

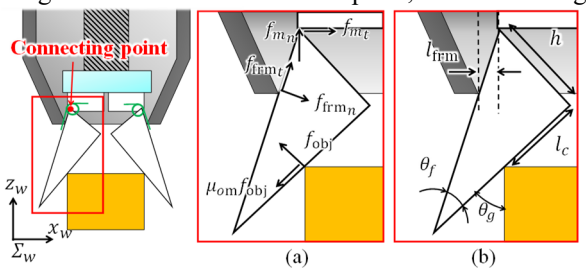

Figure 16. Model for deriving maximum holding force and payload; (a) static and (b) geometrical representations.

where each unilateral arrow at Fig. 16(a) shows the positive direction for each corresponding variable. Note that f_{obj} corresponds to the grasping force, and μ_{om} is the maximum static frictional coefficient (Table II), and θ_f denotes the tip/taper angle of the finger. By considering the instant when sliding occurs at the contact point between the object and the finger, the optimal problem for deriving maximum f_{obj} is given by

$$\begin{aligned} f_{\text{obj}_{\max}} &= \max_{\boldsymbol{f}_g} f_{\text{obj}} \\ \text{Subject to} \quad & \boldsymbol{A}\boldsymbol{f}_g = \boldsymbol{k} \\ & \begin{bmatrix} 0 & 0 & -\mu_{\text{frm}} & -1 & 0 \\ 0 & 0 & -\mu_{\text{frm}} & 1 & 0 \end{bmatrix} \boldsymbol{f}_g \leq \boldsymbol{0} \\ & f_m/3 \geq f_{m_n} \geq 0, \quad f_{\text{frm}_n} \geq 0, \quad f_{\text{obj}} \geq 0 \end{aligned} \tag{10}$$

where

$$\boldsymbol{A} = \begin{bmatrix} 1 & 0 & -S_{gf} & C_{gf} & -\mu_{\text{om}}C_g + S_g \\ 0 & 1 & C_{gf} & S_{gf} & -\mu_{\text{om}}S_g - C_g \\ 0 & 0 & -l_{\text{frm}}/S_{gf} & 0 & h\mu_{\text{om}} + l_c \end{bmatrix}$$

$$\boldsymbol{k} = [0,0,-k\theta_g]^{\text{T}}$$

$$\boldsymbol{f}_g = [f_{m_n}, f_{m_t}, f_{\text{frm}_n}, f_{\text{frm}_t}, f_{\text{obj}}]^{\text{T}}$$

and $S_g = \sin\theta_g$, $C_g = \cos\theta_g$, $S_{gf} = \sin(\theta_g - \theta_f)$, $C_{gf} = \cos(\theta_g - \theta_f)$.

If we utilize $3f_{\text{obj}_{\max}}(\mu_{\text{om}}C_g - S_g)$ as the criterion function, we can get the maximum payload. Because $\mu_{\text{om}}C_g - S_g$ is constant, there is no essential difference in formulation. The fist constraint $\boldsymbol{A}\boldsymbol{f}_g = \boldsymbol{k}$ represents the equilibrium of the force and moment at the connecting point, and $-k\theta_g$ represents the restored torque at the torsion spring. The direction of $\mu_{\text{om}}f_{\text{obj}}$ was derived by considering the sliding direction at the instant when sliding occurs [27]. Please see Fig. 16 for the definitions of the other variables. The second constraint represents the frictional condition at the contact point between the finger and the inside of the cover, and μ_{frm} is the frictional coefficient at the contact point. The third constraint represents the unilaterality of the normal force at each contact point and the maximum load applicable to the feed screw $f_{m_n} \leq f_f/3$. From the Motosh equation [28], the relation between the fastening torque τ_f and the load applied to the fastener f_f at the feed screw is given by

$$\tau_f = \frac{f_f}{2}\left(\frac{\mu_s d_{M10}}{\cos\alpha_s} + \frac{p}{\pi}\right) \tag{11}$$

where $\mu_s = 0.2$ is the frictional coefficient in threads, $d_{M10} = 9.026$ mm is the effective diameter of thread contact, $\alpha_s = 30°$ is the half angle of thread form, and $p = 1.5$ mm is the thread pitch. It is noted that there is no head at feed screw mechanism and the term for the head is then removed at (11). Because $\tau_f = 2000$ Nmm, $f_f = 1560$ N.

We calculated $f_{\text{obj}_{\max}}$ for $\theta_g = 0°\text{–}60°$. Fig. 17 shows the result when $h = 25$ mm, $\mu_{\text{om}} = 0.4$, $l_c = 40$ mm, and $l_{\text{frm}} = 5$ mm. Note that $\mu_{\text{om}} > \mu_k$ because μ_{om} is the static coefficient.

TABLE II. DEFINITION OF THE FRICTIONAL COEFFICIENTS

μ_k	Kinetic frictional coefficient between the object and fingers	μ_o	Ratio of the static frictional force to the normal force between the object and fingers. Maximum value is μ_{om}	μ_r	Ratio of the static frictional force to the normal force between the object and table. Maximum value is μ_{rm}	μ_{frm}	Maximum static frictional coefficient at the contact point between the finger and the inside of the cover

If we consider the case when $\theta_g = 0°$, which corresponds to the normal mode, $f_{\mathrm{obj}_{\max}} = 347$ N and the maximum payload is $3f_{\mathrm{obj}_{\max}}(\mu_{\mathrm{om}}C_g - S_g) = 416$ N (42 kgf). If assuming that the knurl, which provides a high friction, is utilized in the expanded mode, $f_{\mathrm{obj}_{\max}} = 113$ N with setting $\mu_{\mathrm{om}} = 2.0$ and $\theta_g = 60°$, and the maximum payload is $3f_{\mathrm{obj}_{\max}}(\mu_{\mathrm{om}}C_g - S_g) = 45$ N (4.6 kgf).

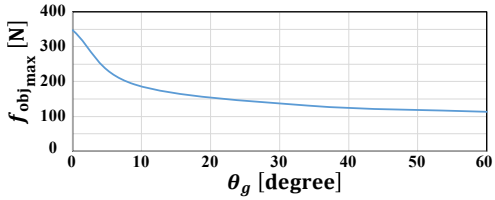

Figure 17. Opening angle θ_g versus maximum holding force $f_{\mathrm{obj}_{\max}}$

B. Experimental validation

Here, we experimentally investigated the maximum payload when grasping an object with the styles shown in Fig. 18. For comparison, we investigated the payload in different loading directions: $+x_w$ direction for the styles 1 and 3 while $-z_w$ direction in the styles 2, 4 and 5. The styles 1 and 3 correspond to the one analyzed in the previous section. We fixed the gripper, grasped the object with a motor torque of 2000 Nmm, and stopped the power supply to the motor. After attaching the grasped object to the plastic container can, water was poured into the can until the object fell down. We measured the weight of the can, including the amount of water when the object fell. The maximum weight of the can with water was 225 N (23 kgf). The target objects for the normal mode were a cylinder (diameter: 20 mm, length: 70 mm) and square rod (20 × 20 × 70 mm), while that for the expanded mode was a cylinder (diameter: 90 mm, length: 30 mm). The examination was conducted five times for each object except for the style 4 (three times). The lowest fingertip always broke off at the style 4 and then we stopped the experiment after the third times of the experiment for safety reason. Table III shows the results. If focusing on the normal mode, in the style 1, the maximum payload was over 225 N (23 kgf), which is the maximum weight of the can with water. In the style 2, the maximum payload was over 15 kgf. If focusing on the expanded mode, the maximum payload was 52.1 N (5.3 kgf) on average in style 3, while 4.9 and 4.2 kgf in styles 4 and 5.

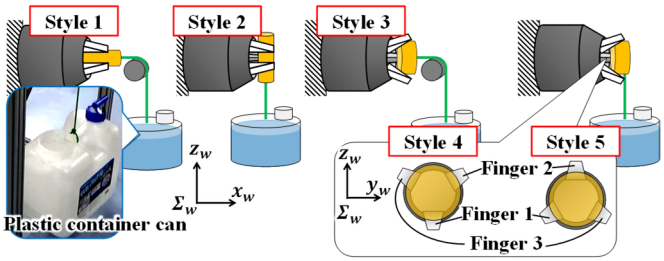

Figure 18. System setup for measurement of resistible load

TABLE III EXPERIMENTAL RESULTS FOR RESISTIBLE LOAD

	Style						
	Normal mode				Expanded mode		
	1		2		3	4	5
	C*	S**	C	S	LC***	LC	LC
Average [N (kgf)]	225 (23)	225 (23)	152 (16)	174 (18)	52.1 (5.3)	47.5 (4.9)	40.8 (4.2)
Standard deviation	0	0	13.6	24.5	12.3	2.45	3.75

* C: Cylinder (D: 20, L: 70mm), ** S: Square rod ($20^2 \times 70$ mm),
*** LC: Large Cylinder (D: 90, L: 70 mm)

V. Grasping And Operation Tests

A. Grasping test

This section presents the results of the grasping test where we tried to grasp several industrial products. The items were initially placed on a table or inside a basin or cup, and then grasped manually. Figs. 1 and 19 show the representative results of the grasping test, which demonstrate the efficacy of the developed gripper (see also attachment video clip).

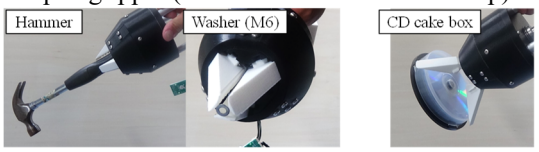

(a) Normal mode (b) Expanded mode
Figure 19. Representative results of the grasping test

B. Operation test

In order to determine whether the developed gripper can be utilized in practical operations, the following four operations were conducted utilizing the gripper: 1) cutting a wooden board by a saw, 2) hammering a nail, 3) tightening an M6 screw with a torque of 5 Nm by a torque wrench and 4) picking up a 2-L PET bottle of water from a corrugated carton. Note that the manipulation was manually conducted. Fig. 20 shows an example of the results demonstrating the efficacy of the gripper (see also attachment video clip).

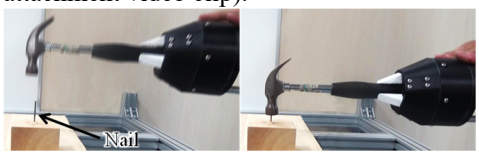

Figure 20. Examples of the operation tests; Hammering a nail

VI. Discussion

The five functional requirements of the gripper design were defined in Section II. We determined that requirements 4 (automatic position and posture alignments) and 5 (cylindrical parts are graspable) were satisfied as discussed in sections III and IV. The maximum payload was over 23 kgf in the normal mode, while the weight of the developed gripper was 0.9 kg; thus, requirements 1 and 2 were also satisfied. An expanded mode was created to facilitate the grasping of wide objects. The CD cake box, shown in Fig. 19(b), was grasped by the gripper in the expanded mode and had a width of 130 mm. This result demonstrates that requirement 3 was satisfied.

The experimental results shown in section III validated the design of the angle of the bevel based on (5) for the position alignment, as well as the control strategy based on (7) for the posture alignment. The maximum load values obtained by the analysis in section IV.A were close to the values obtained by the experiments for styles 1 and 3 in section IV.B. It indicates the validity of the presented approach. From the experimental results for style 2, 4, and 5, it can be seen that the maximum payload in the lateral direction decreased to over 15 and 4 kgf

in the normal and expanded modes, respectively. The decreasing amount in the expanded mode was small comparing to the normal mode. The knurl can locally envelop an object and then the friction force can generate in a wide range of directions. Additionally, the object could get stuck at the knurl. This might be the reason for the small difference. The payload for the expanded mode was small but enough large if considering the payload of manipulator. We conducted the assembly task with the expanded mode (see attachment video clip). The task simulates the assembly task of Robotic Grasping and Manipulation Competition @ IROS 2017. The successful smooth gear (680g) insertion validated the efficacy of the expanded mode.

This paper didn't focus on the operation speed, but the speed-up is often required in industrial fields. The high force is generated by the fastening torque of the feed screw and 2 Nm is required to operate the feed screw. Therefore, any motor that can generate over 2 Nm can be adopted. The maximum closing speed of the developed gripper was 0.8 mm/sec and the minimum closing time was 25.5 s. The operation speed can increase with a higher power motor, although the total weight could increase. An operation, where a required closing distance at a grasping motion is small, is preferable for the gripper. Motion planning including manipulator can make the required closing distance small. Furthermore, an assembly operation and operation utilizing tools are preferable because at these operations, position and posture alignment ability and high grasping force are more important than grasping speed. The size of the gripper is large and a large motion is required for a manipulator to conduct operations. The size reduction is possible but the maximum payload would decrease. The size should be selected based on a given task.

VII. Conclusion

This paper presents a novel gripper for industrial applications, such as part transferring and assembly. The main features of the gripper are its lightweight and high force. The developed gripper was inspired by a chuck clamping device, and the fingers are pushed out by a feed screw mechanism and an outer cover restraint. The developed three-jaw gripper has another feature; the automatic alignment function of its position and posture via a grasping motion. We presented a design criterion for the angle of the bevel for realizing the position alignment as well as a control strategy of gripper velocity for realizing the posture alignment irrespective of an aligned posture. These three features were evaluated analytically and experimentally. Future work will involve the development of autonomous operation methodologies utilizing the developed gripper.

Reference

[1] Mitsubishi electric, "Multifunctional Electric Hand," *[Online]. Available: http://www.mitsubishielectric.com/fa/products/rbt/robot/pmerit/option/hand/index.html#pageUnit01.* .

[2] Schunk, "PZN-plus," *[Online]. Available: http://www.swt.co.kr/file/schunk/PZN-plus_gesamt_EN.pdf.* .

[3] M. Controzzi, C. Cipriani, and M. C. Carrozza, "Design of Artificial Hands: A Review," 2014, pp. 219–246.

[4] G. Hirzinger, J. Butterfass, M. Fischer, M. Grebenstein, M. Hahnle, H. Liu, I. Schaefer, and N. Sporer, "A mechatronics approach to the design of light-weight arms and multifingered hands," *Proc. Millenn. IEEE Int. Conf. Robot. Autom. Symp. Proc.* vol. 1, pp. 46–54, 2000.

[5] J. Butterfass, M. Fischer, M. Grebenstein, S. Haidacher, and G. Hirzinger, "Design and experiences with DLR hand II," *World Autom. Congr. Proc. Tenth Int. Symp. Robot. with Appl.*, pp. 105–109, 2004.

[6] Robotiq, "3-Finger Adaptive Robot Gripper," *[Online]. Available: http://robotiq.com/en/products/industrial-robot-hand/.* .

[7] W. Townsend, "The BarrettHand grasper – programmably flexible part handling and assembly," *Ind. Robot An Int. J.*, vol. 27, no. 3, pp. 181–188, Jun. 2000.

[8] Barret Technology Inc., "Barret Hand BH8-282," *[Online]. Available: http://www.barrett.com/robot/index.htm.* .

[9] Shadow Robot Company, "Shadow Dexterous Hand," 2015. [Online]. Available: http://www.shadowrobot.com/products/dexterous-hand/.

[10] T. Takayama, Y. Chiba, and T. Omata, "Tokyo-TECH 100 N Hand : Three-fingered eight-DOF hand with a force-magnification mechanism," in *2009 IEEE Int. Conf. on Robot. Autom.*, pp. 593–598.

[11] SAKE ROBOTICS, "EZGripper Robotic Grippers," *[Online]. Available: http://sakerobotics.com/products2/.* [Online]. Available: http://sakerobotics.com/products2/.

[12] L. U. Odhner, L. P. Jentoft, M. R. Claffee, N. Corson, Y. Tenzer, R. R. Ma, M. Buehler, R. Kohout, R. D. Howe, and a. M. Dollar, "A compliant, underactuated hand for robust manipulation," *Int. J. Rob. Res.*, vol. 33, no. 5, pp. 736–752, 2014.

[13] I. Gaiser, S. Schulz, A. Kargov, H. Klosek, A. Bierbaum, C. Pylatiuk, R. Oberle, T. Werner, T. Asfour, G. Bretthauer, and R. Dillmann, "A new anthropomorphic robotic hand," - *8th IEEE-RAS International Conference on Humanoid Robots*, 2008, pp. 418–422.

[14] J. Hsu, E. Yoshida, K. Harada, and A. Kheddar, "Self-locking Underactuated Mechanism for Robotic Gripper," in *2016 IEEE Int. Conf. on Advanced Intelligent Mechatronics,* 2017, pp. 620–627.

[15] M. Tavakoli, L. Marques, and A. T. De Almeida, "Flexirigid, a novel two phase flexible gripper," *IEEE Int. Conf. Intell. Robot. Syst.*, pp. 5046–5051, 2013.

[16] NAMIKI PRECISION JEWEL CO., "Multiple DOF hand with grasp force higher than 50kgf (in Japanese)," *[Online]. Available: http://www.jst.go.jp/pr/announce/20160307/.* .

[17] T. Nishimura, K. Mizushima, Y. Suzuki, T. Tsuji, and T. Watanabe, "Variable-grasping-mode underactuated soft gripper with environmental contact-based operation," *IEEE Robot. Autom. Lett.*, vol. 2, no. 2, pp. 1164–1171, 2017.

[18] EMPIRE ROBOTICS, "VERSABALL GRIPPER," *[Online]. Available: http://empirerobotics.com/products.* .

[19] M. T. Zhang and K. Goldberg, "Gripper point contacts for part alignment," *IEEE Trans. Robot. Autom.*, vol. 18, no. 6, pp. 902–910, Dec. 2002.

[20] M. T. Zhang and K. Goldberg, "Designing robot grippers: optimal edge contacts for part alignment," *Robotica*, vol. 25, no. 3, pp. 341–349,2007.

[21] K. Harada, K. Nagata, J. Rojas, I. G. Ramirez-Alpizar, W. Wan, H. Onda, and T. Tsuji, "Proposal of a shape adaptive gripper for robotic assembly tasks," *Adv. Robot.*, vol. 30, no. 17–18, pp. 1186–1198, 2016.

[22] H. Dobashi, J. Hiraoka, T. Fukao, Y. Yokokohji, A. Noda, H. Nagano, T. Nagatani, H. Okuda, and K. Tanaka, "Robust grasping strategy for assembling parts in various shapes.," *Adv. Robot.*, vol. 28, no. 15, pp. 1005–1019, 2014.

[23] Y. Hirata, A. Kaisumi, K. Yamaguchi, and K. Kosuge, "Design of handling device for caging and aligning circular objects," in *2011 IEEE Int. Conf. on Robotics and Automation*, 2011, pp. 4370–4377.

[24] K. Yamaguchi, Y. Hirata, A. Kaisumi, and K. Kosuge, "Design of parts handling and gear assembling device," *Proc. - IEEE Int. Conf. Robot. Autom.*, vol. 1, no. c, pp. 2570–2577, 2012.

[25] Yong Yu, K. Takeuchi, and T. Yoshikawa, "Optimization of robot hand power grasps," in *Proceedings. 1998 IEEE International Conference on Robotics and Automation*, 1998, vol. 4, pp. 3341–3347.

[26] T. Yoshikawa, T. Watanabe, and M. Daito, "Optimization of power grasps for multiple objects," in *Proceedings, IEEE International Conference on Robotics and Automation*, 2001, vol. 2, pp. 1786–1791.

[27] T. Omata and K. Nagata, "Rigid body analysis of the indeterminate grasp force in power grasps," *IEEE Trans. Robot. Autom.*, vol. 16, no. 1, pp. 46–54, 2000.

[28] John H. Bickford, *An Introduction to the Design and Behavior of Bolted Joints,* Second edi. 1990.